Light Controllable Electronic Phase Transition in Ionic Liquid Gated Monolayer Transition Metal Dichalcogenides

Qin, Maosen; Han, Xiangyan; Ding, Dongdong; Niu, Ruirui; Qu, Zhuangzhuang; Wang, Zhiyu; Liao, Zhi-Min; Gan, Zizhao; Huang, Yuan; Han, Chunrui

Published in:
Nano Letters

DOI:
10.1021/acs.nanolett.1c01467

Publication date:
2021

NANO LETTERS

pubs.acs.org/NanoLett

Letter

Light Controllable Electronic Phase Transition in Ionic Liquid Gated Monolayer Transition Metal Dichalcogenides

Maosen Qin, Xiangyan Han, Dongdong Ding, Ruirui Niu, Zhuangzhuang Qu, Zhiyu Wang, Zhi-Min Liao, Zizhao Gan, Yuan Huang, Chunrui Han, Jianming Lu,* and Jianting Ye*

Cite This: *Nano Lett.* 2021, 21, 6800–6806

Read Online

ACCESS | Metrics & More | Article Recommendations | Supporting Information

ABSTRACT: Ionic liquid gating has proved to be effective in inducing emergent quantum phenomena such as superconductivity, ferromagnetism, and topological states. The electrostatic doping at two-dimensional interfaces relies on ionic motion, which thus is operated at sufficiently high temperature. Here, we report the *in situ* tuning of quantum phases by shining light on an ionic liquid-gated interface at cryogenic temperatures. The light illumination enables flexible switching of the quantum transition in monolayer WS_2 from an insulator to a superconductor. In contrast to the prevailing picture of photoinduced carriers, we find that in the presence of a strong interfacial electric field conducting electrons could escape from the surface confinement by absorbing photons, mimicking the field emission. Such an optical tuning tool in conjunction with ionic liquid gating greatly facilitates continuous modulation of carrier densities and hence electronic phases, which would help to unveil novel quantum phenomena and device functionality in various materials.

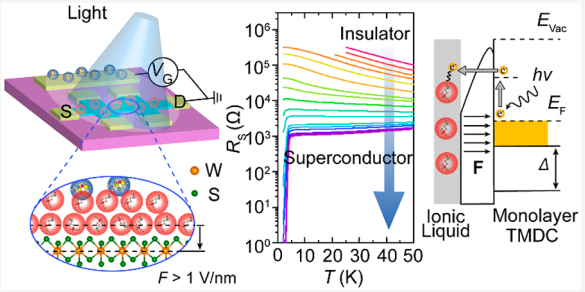

KEYWORDS: *Ionic liquid gating, transition metal dichalcogenides, superconductivity, light illumination, quantum phase transition, field emission*

The electric field control of carrier density is pivotal for uncovering many interesting quantum phenomena such as superconductivity and charge density wave and constructing functional devices. While traditional field-effect transistors (FETs) made of solid dielectrics typically exhibit sheet carrier density n_{2D} around 10^{13} cm^{-2}, the electric-double-layer transistor (EDLT) based on the ionic liquid can accumulate carriers up to 10^{14} or 10^{15} cm^{-2}, which is sufficiently high for accessing various kinds of quantum phases.[1−16] The working principle is straightforward: above the glass transition temperature of ion liquid, the gating electric field drives mobile cations to the sample surface, forming an electric-double layer together with the induced electrons inside the material; as the thickness of the double-layer capacitor is less than 1 nm, the capacitance has orders of enhancement in magnitude.[17] Hence, it was widely applied in material science, contributing to fruitful results. For instance, superconductivity has been induced in many systems, including $SrTiO_3$,[1] ZrNCl,[2] $KTaO_3$,[4] transition metal dichalcogenides (TMDCs),[6−16,18] and so forth. The drawback, however, is that unlike the traditional FETs whose gating voltage could be changed at arbitrary temperatures the EDLT cannot adjust its gating field at low temperatures due to the frozen ionic liquid. Consequently, to characterize a quantum phase transition as a function of doping, multiple ionic liquid gating need to be conducted at a temperature higher than that freezes the ionic motion which is not only time-consuming but, more importantly, might cause inconsistency between electronic states accessed by different ionic gatings. The recent development of the "thermal release" technique extends the operating temperature below the glass transition temperature of ionic liquid.[15] Nevertheless, the highly demanding *in situ* control of quantum phase transition at cryogenic temperature has not been achieved.

Independent of electric gating, light illumination has proved to be possible to tune the carrier density in many systems, such as bare $SrTiO_3$,[19] $SrTiO_3/LaAlO_3$ interface,[20−22] $YBa_2Cu_3O_y$,[23] AlGaN/GaN interface,[24] graphene/BN heterostructures,[25] and graphene/SiO_2 heterostructures.[26,27] The underlying mechanism is that photons activate trapped carriers and increase carrier density. Because of the ultralow recapture rate in certain circumstances, this phenomenon can show persistent photoconductivity. Especially, if the conductance channel is spatially separated from trapping sites (i.e., charged defects), the effect of light illumination resembles the electrostatic gating and the

Received: April 14, 2021
Revised: August 4, 2021
Published: August 9, 2021

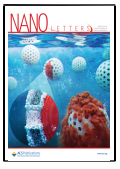

mobility as well as carrier density is significantly enhanced. When applied together with the electric gating field, light illumination has been reported to accelerate interface polarization in $SrTiO_3/LaAlO_3$ interface,[28] or enable charge transfer across TMDCs/graphene hybrid structures,[29,30] or help Fowler-Nordheim tunneling across graphene/boron nitride/graphene heterostructures,[31] which show the promising application of novel-type optoelectronic devices. As the ionic liquid transistor is also endowed with an ultrastrong electric field, the optical stimulus may also provide additional control of carrier density.

In this study, we report light illumination controlled electronic phase transition of monolayer TMDCs in an ionic liquid field-effect transistor. Distinct from the traditional light excitation of trapped charge carriers, we observed that the carrier density is decreased by the illumination, which drives a quantum phase transition from the re-entrant insulating state to an Ising superconductor in monolayer WS_2. Further investigation of its dependence on wavelength and the work function of studied materials suggests a plausible field-emission model, in which photons assist the accumulated electrons in TMDCs to tunnel through the surface potential barrier modified by the strong interfacial electric field between ionic liquid and TMDCs. Our optical stimulus can be operated at cryogenic temperatures when ionic liquid is frozen, which hence exactly compensates for the shortcomings of ionic liquid gating.

We start with the EDLT of monolayer WS_2, a prototypical semiconducting TMDCs. The device structure and measurement scheme are depicted in Figure 1a. The monolayer WS_2 flakes are mechanically exfoliated from bulk crystals and standard electron-beam lithography is followed to make EDLT devices with ionic liquid of *N*,*N*-diethyl-*N*-(2-methoxyethyl)-*N*-methylammonium bis(trifluoromethylsulfonyl-imide) (DEME-TFSI). The light source is a commercial light-emitting diode (LED) and the illumination is conducted either inside cryostats or through an optical window. At 220 K, the gate voltage V_G is scanned between 0 and 6.5 V with a rate of 0.05 V/s (see Supporting Information (SI) Figure 1). During the scanning process, the gate leakage current keeps below 1 nA, excluding any electrochemical reaction (SI Figure 3). After several cycles, we fixed the V_G at 6.5 V and cooled down the device to 80 K immediately. As highlighted by the red arrow in Figure 1c, the monolayer WS_2 is highly doped, entering the re-entrant insulator (as the initial state). It is worth noting that the ions are completely frozen at 80 K, so grounding the gate electrode has no influence on keeping the gating effect. Then at 80 K, the WS_2 sample is exposed to the blue light at $\lambda \sim 462 \pm 15$ nm (0.5 mW). Figure 1b shows the time-dependent sheet resistance R_s under successive illumination. In contrast to the normal photoconductivity caused by exciting electrons from valence to conduction bands, the change of R_s is persistent even after switching off the light. The further distinction can be seen by evaluating the temporal change of R_s as a response to the switching on and off the light illumination, where the expected instantaneous response of photocurrent is lacking (SI Figure 5 and SI Note 2). The remarkable decrease of R_s signifies a dramatic change in electronic states. At each selected exposure time, the temperature dependence of R_s is measured down to 2 K, which is plotted in Figure 1c. An unambiguous re-entrant insulating−superconducting phase transition could be observed when the exposure time increases (see additional high-quality devices on boron nitride flakes in SI Figure 4, where the T_c can reach ∼5 K).

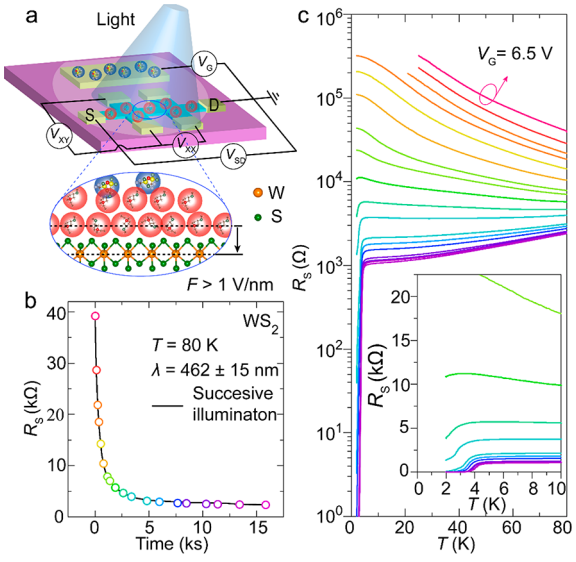

Figure 1. Light controllable electronic phase transition in ionic gated monolayer WS_2. (a) Schematics of an EDLT of monolayer WS_2 exposed to light illumination. Cations ($DEME^+$) and anions ($TFSI^-$) are denoted by red and blue spheres, respectively. Inset: A magnified view of the interface between the monolayer WS_2 and ionic liquid where an electric field in the order of 1 V/nm is established. (b) The sheet resistance R_s of monolayer WS_2 as a function of exposure time under the light of $\lambda \sim 462 \pm 15$ nm at 80 K. The light power is set to be 0.5 mW. (c) Temperature dependence of R_s with various exposure times. Each curve has a correspondence to a circle of the same color in panel (b). As the exposure time increases, a clear insulating phase to the superconducting phase transition is revealed. Inset: Enlarged view of the phase transition in the linear scale.

At first glance, the phase transition to superconductivity could be interpreted by the light excitation of trapped electrons in the localization centers. To check this explanation, Hall measurements were carried out to characterize the evolution of carrier density during the light illumination process (SI Figure 2). Here we focus on the mobile carriers that can be measured by Hall effects of metallic states, since in the re-entrant insulating states the Hall signal is only contributed by the remnant mobile electrons whereas a large portion of electrons is localized and cannot be detected. Also, the linear R_{xy}-B relationship could be well resolved solely in the metallic states at low temperatures while the Hall signal is much noisier in the insulating states. In Figure 2a, two regions of the insulating and superconducting states can be identified by temperature-dependent sheet resistance extracted from Figure 1c. Surprisingly, the carrier density keeps decreasing with increasing exposure time (Figure 2b and SI Figure 2), which is in contrast to the conventional scenario in which more carriers are generated by optically exciting trapped electrons. Concomitantly, the carrier mobility rises gradually (Figure 2b), so does the superconducting critical temperature T_c (Figure 2c). The opposite trend of carrier density and mobility infers that neutral defect scatterings (short-range interaction) dominate the mobility because charged impurity centers (long-range) tend to be screened hence are causing less scattering when the carrier density becomes higher. On the other hand, the positive relation between mobility and T_c suggests the existence of charged defect scattering which is known to renormalize the Coulomb interaction between

https://doi.org/10.1021/acs.nanolett.1c01467
Nano Lett. 2021, 21, 6800−6806

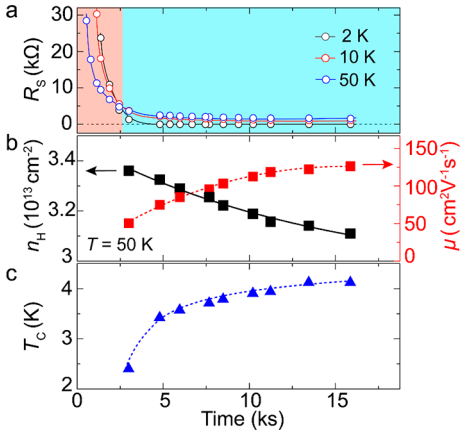

Figure 2. Evolutionary superconducting properties induced by light illumination. (a) The exposure time dependence of R_s at various temperatures, indicating the insulating and superconducting regions color-coded by red and blue, respectively. (b). The Hall carrier density n_H and mobility as a function of the exposure time at 50 K are plotted on the left and right axes, respectively. The former is fitted by a stretched exponential decay law (black solid line). The dashed red line is a guide to the eye. (c) Superconducting critical temperature T_c as a function of the exposure time. T_c is defined at 50% of normal state resistance. The dashed blue line is a guide to the eye.

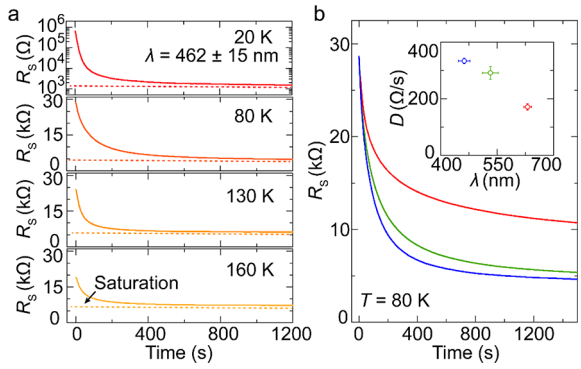

Figure 3. Dependence of light illumination on temperature and wavelength. (a) R_s of monolayer WS_2 as a function of exposure time at 20, 80, 130, and 160 K, respectively. Dashed lines indicate the magnitude of saturated resistance at different temperatures. The exposure time required to saturate does not have a strong temperature dependence. The light used is 462 ± 15 nm and 5 mW. (b) With the light of 462 ± 15, 532 ± 21, and 631 ± 10 nm, R_s of monolayer WS_2 decreases rapidly then tends to saturate. All of the data are taken at 80 K. The light power is set to be 5 mW for each light source. Inset: The illumination efficiency D is defined by the decay rate of R_s in the initial linear range. Horizontal error bars correspond to the half-width of the emission spectra. Vertical error bars are estimated from the uncertainty in the range chosen for the linear fitting.

electrons in Cooper pairs. Overall, mediated by carrier density, light illumination manages to turn the re-entrant insulator directly into superconducting states and achieves fine-tuning of various intrinsic properties of the electronic system.

To gain more insight into the illumination effect, we further check its dependence on temperature and optical wavelength in another similar sample. Here, we add two additional light sources, that is, green ($\lambda \sim 532 \pm 21$ nm) and red ($\lambda \sim 631 \pm 10$ nm), and calibrate the power density for all the three LEDs to quantify the illumination efficiency. Before each illumination, we warmed up the device to 220 K to erase all of the doping effects then cooled down to desired temperatures and repeated the same procedure. Because of the high stability of electrostatic gating of EDLT, we could obtain nearly the same initial state in every cycle of the measurement. In Figure 3a, the wavelength is fixed as 462 ± 15 nm and the temperature is chosen at 20, 80, 130, and 160 K, respectively. Without illumination, the electronic state is found to be insulating: R_s increases from 19 kΩ at 160 K to 660 kΩ at 20 K. After 20 min of exposure, the sample approaches a saturation state that behaves to be metallic (denoted by dashed lines at each temperature): R_s decreases from 7.4 kΩ at 160 K to 1.4 kΩ at 20 K. Although the change of R_s at 20 K is two orders larger than that at 160 K, the sheet resistance versus exposure time shows a similar trend within the wide temperature range. It seems that the temperature difference in the order of 10 meV has no notable influence on the illumination efficiency, which suggests that heating should not play an important role. In contrast, the photon energy may vary in the order of electronvolts in the visible range. Figure 3b shows the sheet resistance versus time with the different wavelengths from 462 to 631 nm. The constant-temperature measurement (80 K) enables direct comparison of the illumination efficiency defined by $D = \Delta R_s/\Delta t$, which could be extracted within the linear region at the beginning of the exposure. As shown in the inset of Figure 3b, illuminating with photons of higher energy clearly causes a faster decrease in the resistance. Note that it is the red light, rather than the blue one, that has energy close to the direct exciton of WS_2 around 2.1 eV.[32] This may indicate that the resonant absorption is not intimately related to the mechanism of the illumination effect. Furthermore, the photoconductivity generated from the optical excitation shows no influence on the illumination effect, which is probably overwhelmed by the high electron doping in the WS_2 (see SI Figure 5).

So far, we have been limited to the metallic region for the analysis of carrier density, due to the difficulty to get carrier density in the strong insulating state of monolayer WS_2. To evaluate the illumination effect in a wider range of ionic liquid gating, in the following we examine the EDLT of MoS_2 that has very weak insulating behavior. Under the successive blue light illumination, R_s of MoS_2 can be also effectively modulated, similar to the performance of WS_2 (Figure 4a). As shown in Figure 4c, the temperature-dependent R_s is measured with different exposure time, where a re-entrant insulating to metallic phase transition could be identified. The absence of the superconductivity in all the metallic states is probably due to the low T_c of monolayer MoS_2 that has been reported to be lower than our base temperature.[13,18] Thanks to the very weak insulator, the linear R_{xy}–B relationship can be obtained across the whole gating range at low temperatures. As shown in Figure 4b, the carrier density as a function of exposure time is qualitatively similar to that in WS_2, although the magnitude of carrier density and its variation are nearly three times larger in MoS_2 (see SI Figure 2). As for mobility, a similar trend with exposure time can be observed. Consequently, we can now conclude that the light illumination universally decreases carrier density in EDLT of monolayer TMDCs

To understand the unusual dependence of the carrier density on light illumination, here we tentatively understand it with a photon-assisted field emission model. In the presence of the extremely strong interfacial electric field reaching over 1 V/nm, the surface barrier of monolayer TMDCs in the real space

https://doi.org/10.1021/acs.nanolett.1c01467
Nano Lett. 2021, 21, 6800−6806

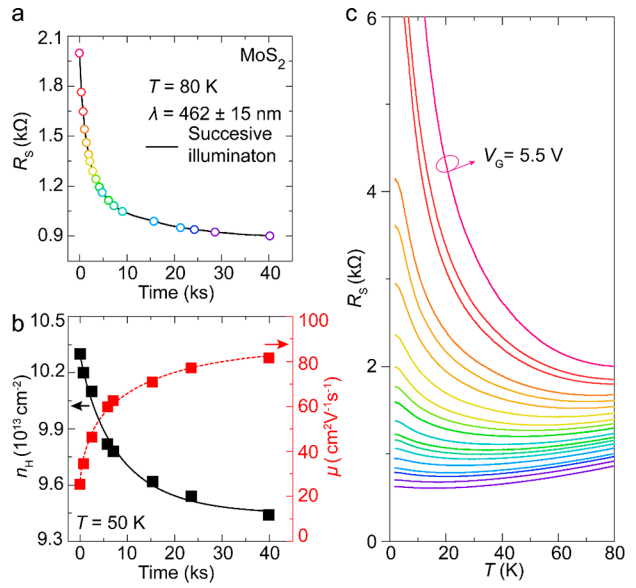

Figure 4. Light illumination on ionic gated monolayer MoS_2. (a) R_s of monolayer MoS_2 as a function of exposure time with the light of 462 ± 15 nm at 80 K. The light power intensity is set to be 0.5 mW. (b) The Hall carrier density n_H and mobility as a function of exposure time at 50 K are plotted to the left and right axes, respectively. n_H is fitted by a stretched exponential decay law (black solid line). The dashed red line is a guide to the eye. (c) Temperature dependence of R_s with various exposure times. Each curve corresponds to a circle of the same color in (a). Note the initial state is only weakly insulating and no superconductivity is observed above 2 K.

is significantly modified (see the rounded triangular shape in Figure 5a) and can be expressed as

$$\phi = \Delta\phi - eFx - \frac{e^2}{16\pi\varepsilon_0 x} \tag{1}$$

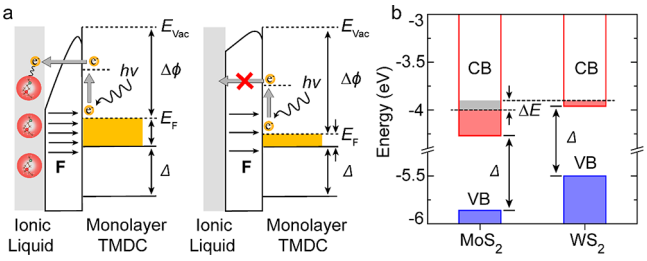

Figure 5. Photon-assisted field emission model in the ionic liquid transistor. (a) Strong interfacial electric field F reshapes the potential barrier into a rounded triangle, which greatly enhances the tunneling probability of electrons that have absorbed photon energy (left panel). Because of the atomic thickness, band edges of monolayer TMDCs are denoted by an energy level without bending. When the carrier density is low, the Fermi level E_F decreases and so does the field strength F. Consequently, the tunneling process is suppressed and the resistance/carrier density saturates (right panel). $\Delta\phi$: the energy difference between E_F and the vacuum level E_{vac}. (b) The magnitudes of $\Delta\phi$ (dashed line) in saturation states are compared for MoS_2 and WS_2. The conduction and valence band edge and band gap are also indicated referring to the vacuum level E_{vac}. The red filling denotes the band filling by remnant electrons, which are distinct for MoS_2 and WS_2, leading to different electric fields and hence surface potential barriers. The energy difference denoted by the gray color (ΔE) is approximately equal to that of $\Delta\phi$ in these two materials (see text).

where $\Delta\phi$ is the energy difference between the Fermi level E_F and the vacuum level E_{vac}, F is the interfacial electric field, ε_0 is the vacuum permittivity, e is the elementary charge, and x is the distance from TMDCs. The electron tunneling probability, described by the celebrated Fowler–Nordheim (FN) law adapted for a 2D planar electron emitter,[33,34] could be written as

$$P \propto \exp\left(-\frac{\beta}{F}\right) \tag{2}$$

where $\beta = \frac{4\sqrt{2m}\left(\phi - \frac{h\upsilon}{2}\right)^{3/2}}{3e\hbar}$, m is the effective mass, $h\upsilon$ is the photon energy, and $\hbar$ is the reduced Planck's constant. Qualitatively, as shown by the left panel of Figure 5a, assisted by photons of several electronvolts, electrons would have sufficient energy to tunnel through the triangular surface potential barrier and are subsequently captured by positively charged ions (i.e., neutralization) in the ionic liquid. Hence, the effective charges within the electric double layer, that is, the density of cations on the left and electrons on the right side of the potential barrier, start to decrease, which in turn weakens the electric field F that shapes the surface potential barrier. As a result, the tunneling probability decays exponentially. With a long time of light exposure, we finally reach the situation indicated in the right panel of Figure 5a in which residual electrons in the conduction band are prohibited to tunnel through the nearly unmodified potential. Therefore, the illumination effect is suppressed and both R_s and n_H saturate.

More quantitatively, we could examine the model by comparing the saturation state between MoS_2 and WS_2. First, we find the exposure time-dependent carrier density could be well fitted by Kohlrausch formulizm which usually describes complex systems approaching equilibrium[35,36]

$$\frac{n_H(t) - n_s}{n_H(0) - n_s} = \exp[-(t/\tau)^\alpha] \tag{3}$$

where τ, α, and n_s stand for the exponential decay time, the decay exponent ($0 < \alpha < 1$), and the saturation-state carrier density, respectively. The fitting could also be justified by considering that the electronic system exposed to light is not in equilibrium, which is consistent with the literature.[37,38] The fitting parameter n_s are 9.44×10^{13} and 2.92×10^{13} cm^{-2} for MoS_2 and WS_2, respectively (see fitting curves in Figure 2b and Figure 4b). Then we could estimate $\Delta\phi$ in eq 1. As the band structure of monolayer TMDCs is well documented, the 2D DOS ($\frac{m}{2\pi\hbar^2}$) associated with different valleys could be directly calculated with valley degeneracy and effective mass.[39] Hence, we can reliably obtain corresponding Fermi levels E_F for the above saturation states (see SI Table 1). Take theoretical values[40] of work function ϕ_0 (MoS_2, 5.07 eV; WS_2, 4.73 eV), band gap Δ (MoS_2, 1.59 eV; WS_2, 1.54 eV) and Fermi energy E_F, $\Delta\phi = \phi_0 - E_F - \Delta/2$ are calculated to be 4.06 and 3.87 eV for MoS_2 and WS_2, respectively (Figure 5b). The tiny difference of ~190 meV could be attributed to the modification of the surface barrier by different interfacial electric field F. Considering that the tunneling process occurs below ~1 nm in the monolayer TMDCs, we roughly estimate the energy difference between these two surface barriers by using a parallel-plate capacitor $\Delta E = e^2\Delta n/C_{IL}$, where Δn is the difference of n_s in the two materials and C_{IL} is the capacitance of ionic liquid. Using C_{IL} = 20–60 $\mu F/cm^2$,[41–44] we obtain ΔE

https://doi.org/10.1021/acs.nanolett.1c01467
Nano Lett. 2021, 21, 6800–6806

= 173−521 meV, which agrees well with the energy difference in $\Delta\phi$.

Although the above comparison between different materials gives strong evidence of the field emission model, the dependence on optical wavelength is not yet clear on a quantitative level in this model. This is because the determination of the photon energy threshold needs the detailed distribution of electric field within the electric-double layer which is still highly debated. Qualitatively, the light of higher energy should be more efficient to help the tunneling, consistent with experimental results (Figure 3b) where illuminations in blue and green have a much more remarkable decay rate than the red light.

Finally, we would like to briefly discuss the fate of the emitted electrons. The principle of the electric-double layer in the ionic gating suggests that the cations and the induced electrons in the channel should have one-to-one correspondence. As the carrier density is shown to decrease during light illumination, cations must be changed simultaneously.

Capturing an emitted electron in the double layer is expected to passivate a cation. In electrochemistry, it is well-known that when the bias voltage exceeds a certain threshold, cations will obtain electrons from the cathode causing reductive reaction. For ionic liquid, the reduction usually results in the decomposition of cation into fractional molecules.[45,46] In our system, the electron emission occurs at cryogenic temperature at which ionic motion of cations are frozen. It is, therefore, not clear whether the cation has sufficient chemical kinetics to have an immediate chemical reaction. The chemical resilience at lower temperature has been well demonstrated by the significantly enlarged chemical window that allows electrostatic gating at 220 K up to 6.5 V, compared with the commercially specification of ∼3 V at room temperature (SI Figure 3). Considering the high stability, it is possible to accommodate the electrons as unpaired electron mimicking the formation of "color center" in ionic crystals. Here, for frozen ionic liquid at the interface there should be abundant interstitial sites to capture the emitted electrons.

Although the details need further identification (see more discussion about any possible electrochemical reaction in Supporting Information), the scenario of passivating cations agrees with the experimental observation, for instance, the increase of electron mobility during light illumination (Figure 2b and Figure 4b). The dominant scattering with electrons in the ionic liquid transistor is believed to be from nonperiodically distributed cations. Especially, considering that the ions in the double layer may be not uniform in the z-direction, the protruded cations have the strongest electric fields so that these sites that contribute most to the scattering are easier to be passivated. Therefore, despite the decreasing electron density that provides poorer Coulomb screening of cations, the significantly reduced cations and randomness leads to a suppressed scattering rate and hence enhanced mobility.

In conclusion, we have observed an unusual light illumination effect, which directly controls the electronic phase transition from the re-entrant insulating to the superconducting state in the ionic gated monolayer TMDCs at cryogenic temperatures. Also, a photon-assisted field emission model is provided to tentatively reconcile our experimental results on both WS_2 and MoS_2 samples. The light illumination established here could be extended to a wide variety of ionic gated systems, pioneering a new method to continuously control the electronic phase transition by tuning the carrier density. Moreover, the monolayer TMDCs based EDLT integrated with optical modulation shows a high efficiency on the switching from nonconductive states to superconductors, which may bring broad prospects for device applications.

■ ASSOCIATED CONTENT

Supporting Information

The Supporting Information is available free of charge at https://pubs.acs.org/doi/10.1021/acs.nanolett.1c01467.

Materials includes detailed discussion of the field emission model, the effect of photoconductivity, basic characterization of EDLT devices such as transfer curves and Hall effects, stability in multiple cycles of electrostatic gating, temporal change of resistances during light illumination, measurements of an additional sample on the h-BN substrate, calculation details of Fermi level in doped monolayer MoS_2 and WS_2 (PDF)

■ AUTHOR INFORMATION

Corresponding Authors

Jianming Lu − *State Key Laboratory for Mesoscopic Physics, School of Physics, Peking University, Beijing 100871, China;* orcid.org/0000-0002-1558-4040; Email: jmlu@pku.edu.cn

Jianting Ye − *Device Physics of Complex Materials, Zernike Institute for Advanced Materials, University of Groningen, Groningen 9746AG, The Netherlands;* Email: j.ye@rug.nl

Authors

Maosen Qin − *State Key Laboratory for Mesoscopic Physics, School of Physics, Peking University, Beijing 100871, China;* orcid.org/0000-0001-8681-2584

Xiangyan Han − *State Key Laboratory for Mesoscopic Physics, School of Physics, Peking University, Beijing 100871, China*

Dongdong Ding − *State Key Laboratory for Mesoscopic Physics, School of Physics, Peking University, Beijing 100871, China*

Ruirui Niu − *State Key Laboratory for Mesoscopic Physics, School of Physics, Peking University, Beijing 100871, China*

Zhuangzhuang Qu − *State Key Laboratory for Mesoscopic Physics, School of Physics, Peking University, Beijing 100871, China*

Zhiyu Wang − *State Key Laboratory for Mesoscopic Physics, School of Physics, Peking University, Beijing 100871, China*

Zhi-Min Liao − *State Key Laboratory for Mesoscopic Physics, School of Physics and Frontiers Science Center for Nano-optoelectronics, School of Physics, Peking University, Beijing 100871, China; Yangtze Delta Institute of Optoelectronics, Peking University, Nantong, Jiangsu 226010, China;* orcid.org/0000-0001-6361-9626

Zizhao Gan − *State Key Laboratory for Mesoscopic Physics, School of Physics, Peking University, Beijing 100871, China*

Yuan Huang − *Institute of Physics, , Chinese Academy of Sciences, Beijing 100190, China*

Chunrui Han − *Institute of Microelectronics, Chinese Academy of Sciences, Beijing 100029, China*

Complete contact information is available at: https://pubs.acs.org/10.1021/acs.nanolett.1c01467

Notes

The authors declare no competing financial interest.

https://doi.org/10.1021/acs.nanolett.1c01467
Nano Lett. 2021, 21, 6800−6806

■ ACKNOWLEDGMENTS

J.M.L. acknowledges supports from NSFC No. 11974027, National Key R&D Program of China No. 2019YFA0307800, and Beijing Natural Science Foundation No. Z190011. J.Y. is supported by European Research Council (consolidator Grant 648855 Ig-QPD). Y.H. is supported by National Key R&D Program of China No. 2019YFA0308000, NSFC 11874405, and the Youth Innovation Promotion Association of CAS (2019007). Z.M.L. is supported by NSFC 61825401 and National Key R&D Program of China No. 2018YFA0703703.

■ REFERENCES

(1) Ueno, K.; et al. Electric-field-induced superconductivity in an insulator. *Nat. Mater.* **2008**, *7*, 855−858.
(2) Ye, J. T.; et al. Liquid-gated interface superconductivity on an atomically flat film. *Nat. Mater.* **2010**, *9*, 125−128.
(3) Bollinger, A. T.; et al. Superconductor−insulator transition in $La_{2-x}Sr_x$ CuO_4 at the pair quantum resistance. *Nature* **2011**, *472*, 458−460.
(4) Ueno, K.; et al. Discovery of superconductivity in $KTaO_3$ by electrostatic carrier doping. *Nat. Nanotechnol.* **2011**, *6*, 408−412.
(5) Ye, J.; et al. Accessing the transport properties of graphene and its multilayers at high carrier density. *Proc. Natl. Acad. Sci. U. S. A.* **2011**, *108*, 13002−13006.
(6) Ye, J. T.; et al. Superconducting Dome in a Gate-Tuned Band Insulator. *Science* **2012**, *338*, 1193−1196.
(7) Jo, S.; Costanzo, D.; Berger, H.; Morpurgo, A. F. Electrostatically Induced Superconductivity at the Surface of WS_2. *Nano Lett.* **2015**, *15*, 1197−1202.
(8) Yu, Y.; et al. Gate-tunable phase transitions in thin flakes of 1T-TaS_2. *Nat. Nanotechnol.* **2015**, *10*, 270−276.
(9) Saito, Y.; Kasahara, Y.; Ye, J.; Iwasa, Y.; Nojima, T. Metallic ground state in an ion-gated two-dimensional superconductor. *Science* **2015**, *350*, 409−413.
(10) Shi, X.; Li, X.; Jiang, L.; Qu, L.; Zhao, Y.; Ran, P.; Wang, Q.; Cao, Q.; Ma, T.; Lu, Y. Superconductivity Series in Transition Metal Dichalcogenides by Ionic Gating. *Sci. Rep.* **2015**, *5*, 12534.
(11) Lu, J. M.; et al. Evidence for two-dimensional Ising superconductivity in gated MoS_2. *Science* **2015**, *350*, 1353−1357.
(12) Li, L. J.; et al. Controlling many-body states by the electric-field effect in a two-dimensional material. *Nature* **2016**, *529*, 185−189.
(13) Costanzo, D.; Jo, S.; Berger, H.; Morpurgo, A. F. Gate-induced superconductivity in atomically thin MoS_2 crystals. *Nat. Nanotechnol.* **2016**, *11*, 339−344.
(14) Xi, X.; Berger, H.; Forró, L.; Shan, J.; Mak, K. F. Gate Tuning of Electronic Phase Transitions in Two-Dimensional $NbSe_2$. *Phys. Rev. Lett.* **2016**, *117*, 106801.
(15) Lu, J.; et al. Full superconducting dome of strong Ising protection in gated monolayer WS_2. *Proc. Natl. Acad. Sci. U. S. A.* **2018**, *115*, 3551−3556.
(16) Costanzo, D.; et al. Tunnelling spectroscopy of gate-induced superconductivity in MoS_2. *Nat. Nanotechnol.* **2018**, *13*, 483−488.
(17) Kötz, R.; Carlen, M. Principles and applications of electrochemical capacitors. *Electrochim. Acta* **2000**, *45*, 2483−2498.
(18) Fu, Y.; Liu, E.; Yuan, H.; Tang, P.; Lian, B.; Xu, G.; Zeng, J.; Chen, Z.; Wang, Y.; Zhou, W.; Xu, K.; Gao, A.; Pan, C.; Wang, M.; Wang, B.; Zhang, S.-C.; Cui, Y.; Hwang, H. Y.; Miao, F. Gated tuned superconductivity and phonon softening in monolayer and bilayer MoS_2. *npj Quant. Mater.* **2017**, *2*, 52.
(19) Tarun, M. C.; Selim, F. A.; McCluskey, M. D. Persistent Photoconductivity in Strontium Titanate. *Phys. Rev. Lett.* **2013**, *111*, 187403.
(20) Rastogi, A.; Budhani, R. C. Solar blind photoconductivity in three-terminal devices of $LaAlO_3$/$SrTiO_3$ heterostructures. *Opt. Lett.* **2012**, *37*, 317.
(21) Su, S.; Gao, H.; Shen, Y.; Peng, W.; Zhu, X. Visible-light-mediated carrier type modulation at the $LaAlO_3$ /$SrTiO_3$ interface. *Appl. Phys. Lett.* **2019**, *115*, 151601.
(22) Tebano, A.; Fabbri, E.; Pergolesi, D.; Balestrino, G.; Traversa, E. Room-Temperature Giant Persistent Photoconductivity in $SrTiO_3$ /$LaAlO_3$ Heterostructures. *ACS Nano* **2012**, *6*, 1278−1283.
(23) Tanabe, K.; Kubo, S.; Hosseini Teherani, F.; Asano, H.; Suzuki, M. Effects of photoinduced hole doping on normal-state and superconducting transport in oxygen-deficient $YBa_2Cu_3O_y$. *Phys. Rev. Lett.* **1994**, *72*, 1537−1540.
(24) Li, J. Z.; Lin, J. Y.; Jiang, H. X.; Asif Khan, M.; Chen, Q. Persistent photoconductivity in a two-dimensional electron gas system formed by an AlGaN/GaN heterostructure. *J. Appl. Phys.* **1997**, *82*, 1227−1230.
(25) Ju, L.; et al. Photoinduced doping in heterostructures of graphene and boron nitride. *Nat. Nanotechnol.* **2014**, *9*, 348−352.
(26) Kim, Y. D.; et al. Focused-Laser-Enabled p−n Junctions in Graphene Field-Effect Transistors. *ACS Nano* **2013**, *7*, 5850−5857.
(27) Tiberj, A.; Rubio-Roy, M.; Paillet, M.; Huntzinger, J. -R.; Landois, P.; Mikolasek, M.; Contreras, S.; Sauvajol, J. -L.; Dujardin, E.; Zahab, A. -A. Reversible optical doping of graphene. *Sci. Rep.* **2013**, *3*, 2355.
(28) Lei, Y.; et al. Visible-light-enhanced gating effect at the $LaAlO_3$/$SrTiO_3$ interface. *Nat. Commun.* **2014**, *5*, 5554.
(29) Roy, K.; et al. Graphene−MoS_2 hybrid structures for multifunctional photoresponsive memory devices. *Nat. Nanotechnol.* **2013**, *8*, 826−830.
(30) Yu, W. J.; et al. Highly efficient gate-tunable photocurrent generation in vertical heterostructures of layered materials. *Nat. Nanotechnol.* **2013**, *8*, 952−958.
(31) Ma, Q.; et al. Tuning ultrafast electron thermalization pathways in a van der Waals heterostructure. *Nat. Phys.* **2016**, *12*, 455−459.
(32) Mak, K. F.; Shan, J. Photonics and optoelectronics of 2D semiconductor transition metal dichalcogenides. *Nat. Photonics* **2016**, *10*, 216−226.
(33) Ang, Y. S.; Zubair, M.; Ooi, K. J. A. et al. Generalized Fowler-Nordheim field-induced vertical electron emission model for two-dimensional materials. arXiv, 2017, 1711.05898 [cond-mat.mes-hall].https://arxiv.org/abs/1711.05898 (accessed Nov 16, 2017).
(34) Ang, Y. S.; Cao, L.; Ang, L. K. Physics of electron emission and injection in two-dimensional materials: Theory and simulation. *InfoMat* **2021**, *3*, 502.
(35) Chamberlin, R. V.; Mozurkewich, G.; Orbach, R. Time Decay of the Remanent Magnetization in Spin-Glasses. *Phys. Rev. Lett.* **1984**, *52*, 867−870.
(36) Palmer, R. G.; Stein, D. L.; Abrahams, E.; Anderson, P. W. Models of Hierarchically Constrained Dynamics for Glassy Relaxation. *Phys. Rev. Lett.* **1984**, *53*, 958−961.
(37) Li, B. K.; Wang, C.; Sou, I. K.; Ge, W. K.; Wang, J. N. Anomalous photocurrent observed in an Fe−ZnS:Fe Schottky diode. *Appl. Phys. Lett.* **2007**, *91*, 172104.
(38) Kall, M.; Osada, M.; Kakihana, M.; Borjesson, L.; Frello, T.; Madsen, J.; Andersen, N. H.; Liang, R.; Dosanjh, P.; Hardy, W. N. CuO-chain Raman scattering and photoinduced metastability in $YBa_2Cu_3O_x$. *Phys. Rev. B: Condens. Matter Mater. Phys.* **1998**, *57*, 072−075.
(39) Kormányos, A.; et al. $\mathbf{k} \cdot \mathbf{p}$ theory for two-dimensional transition metal dichalcogenide semiconductors. *2D Mater.* **2015**, *2*, 022001.
(40) Gong, C.; et al. Band alignment of two-dimensional transition metal dichalcogenides: Application in tunnel field effect transistors. *Appl. Phys. Lett.* **2013**, *103*, 053513.
(41) Fujimoto, T.; Awaga, K. Electric-double-layer field-effect transistors with ionic liquids. *Phys. Chem. Chem. Phys.* **2013**, *15*, 8983.
(42) Ono, S.; Miwa, K.; Seki, S.; Takeya, J. A comparative study of organic single-crystal transistors gated with various ionic-liquid electrolytes. *Appl. Phys. Lett.* **2009**, *94*, 063301.
(43) Kim, S. H.; et al. Electrolyte-Gated Transistors for Organic and Printed Electronics. *Adv. Mater.* **2013**, *25*, 1822−1846.

https://doi.org/10.1021/acs.nanolett.1c01467
Nano Lett. 2021, 21, 6800−6806

(44) Bisri, S. Z.; Shimizu, S.; Nakano, M.; Iwasa, Y. Endeavor of Iontronics: From Fundamentals to Applications of Ion-Controlled Electronics. *Adv. Mater.* **2017**, *29*, 1607054.
(45) Lane, G. H. Electrochemical reduction mechanisms and stabilities of some cation types used in ionic liquids and other organic salts. *Electrochim. Acta* **2012**, *83*, 513−528.
(46) Kroon, M. C.; Buijs, W.; Peters, C. J.; Witkamp, G. J. Decomposition of ionic liquids in electrochemical processing. *Green Chem.* **2006**, *8*, 241−245.

https://doi.org/10.1021/acs.nanolett.1c01467
Nano Lett. 2021, 21, 6800−6806